

# Graph Neural Networks Based Detection of Stealth False Data Injection Attacks in Smart Grids

Osman Boyaci, *Student Member, IEEE*, Amarachi Umunnakwe, *Student Member, IEEE*, Abhijeet Sahu, *Student Member, IEEE*, Mohammad Rasoul Narimani, *Member, IEEE*, Muhammad Ismail, *Senior Member, IEEE*, Katherine Davis, *Senior Member, IEEE*, and Erchin Serpedin, *Fellow, IEEE*

**Abstract**— False data injection attacks (FDIAs) represent a major class of attacks that aim to break the integrity of measurements by injecting false data into the smart metering devices in power grid. To the best of authors' knowledge, no study has attempted to design a detector that automatically models the underlying graph topology and spatially correlated measurement data of the smart grids to better detect cyber attacks. The contributions of this paper to detect and mitigate FDIAs are twofold. First, we present a generic, localized, and stealth (unobservable) attack generation methodology and a publicly accessible dataset for researchers to develop and test their algorithms. Second, we propose a Graph Neural Network (GNN) based, scalable and real-time detector of FDIAs that efficiently combines model-driven and data-driven approaches by incorporating the inherent physical connections of modern AC power grids and exploiting the spatial correlations of the measurement data. It is experimentally verified by comparing the proposed GNN based detector with the currently available FDIA detectors in literature that our algorithm outperforms the best available solutions by 6.21%, 0.69%, and 2.73% in detection rate and by 3.65%, 0.34% and 1.38% in F1 score for standard IEEE testbeds with 14, 118, and 300 buses, respectively.

## NOMENCLATURE

$P_i + jQ_i$	Complex power injection at bus $i$ .
$P_{ij} + jQ_{ij}$	Complex power flow between bus $i$ and $j$ .
$V_i, \theta_i$	Voltage magnitude and phase angle of bus $i$ .
$\theta_{ij}$	$\theta_i - \theta_j$ .
$G_{ij} + jB_{ij}$	$ij$ th elements of bus admittance matrix.
$g_{ij} + jb_{ij}$	Series branch admittance between bus $i$ and $j$ .
$g_{si} + jb_{si}$	Shunt branch admittance at bus $i$ .
$\Omega_i$	Set of buses connected to bus $i$ .
$\mathbf{x} \in \mathbb{R}^n$	A state vector.
$\hat{\mathbf{x}} \in \mathbb{R}^n$	Original state vector without an attack.
$\check{\mathbf{x}} \in \mathbb{R}^n$	False data injected state vector.
$\mathbf{z} \in \mathbb{R}^m$	A measurement vector.
$\mathbf{z}_o \in \mathbb{R}^m$	Original measurement vector.
$\mathbf{z}_a \in \mathbb{R}^m$	Attacked measurement vector.
$h(\mathbf{x})$	Nonlinear measurement function at $\mathbf{x}$ .
$\mathbf{H} \in \mathbb{R}^{m \times n}$	Jacobian matrix.

O. Boyaci, A. Umunnakwe, A. Sahu, M. R. Narimani, K. Davis, and E. Serpedin are with the Department of Electrical and Computer Engineering, Texas A&M University, College Station, TX 77843 USA (e-mail: {osman.boyaci, amarachi, abhijeet\_ntpc, narimani, katedavis, eserpedin}@tamu.edu). M. Ismail is with the Department of Computer Science, Tennessee Tech University, Cookeville, TN 38505 USA (email: mismail@tnstate.edu)

This work was supported by NSF under Award Number 1808064. The data that support the findings of this study are available in <https://katedavis.engr.tamu.edu/projects/defenda/>

$\mathbf{R} \in \mathbb{R}^{m \times m}$  Error covariance matrix.

$\mathbf{G} \in \mathbb{R}^{n \times n}$  Gain matrix.

$\mathbf{S} \in \mathbb{R}^{m \times m}$  Residual sensitivity matrix.

$\mathbf{r} \in \mathbb{R}^m$  Residue vector.

$\mathbf{r}^N \in \mathbb{R}^m$  Normalized residue vector.

$\mathcal{T}$  Attacker's target area to perform FDIA.

$\mathcal{T}_z$  Set of measurements in  $\mathcal{T}$ .

$\mathcal{T}_x$  Set of state variables in  $\mathcal{T}$ .

$\mathfrak{Z}, \mathfrak{X}$  Measurement space, state space.

## I. INTRODUCTION

As a highly complex cyber-physical system, a smart grid consists of a physical power system infrastructure and a cyber communication network. Physical measurement data are first acquired by the Remote Terminal Units (RTUs) or Phasor Measurement Units (PMUs) and are delivered to the Supervisory Control and Data Acquisition Systems (SCADAs). Then, the communication network transfers the measurement data to the application level where are processed and evaluated by the power applications [1]. Consequently, reliability of power system operations heavily depends on the security of the cyber-physical pipeline [2].

Power system state estimation (PSSE) is a highly critical component of this pipeline since its outcome is directly fed into numerous Energy Management System (EMS) blocks such as load and price forecasting, contingency and reliability analysis, and economic dispatch processes [3], [4]. Thus, integrity and trustworthiness of the measurement data play a critical role in ensuring proper operation of smart grids [5]. By breaking this integrity, cyber-physical attacks target smart metering devices to harm the underlying physical systems.

False data injection attacks (FDIAs) represent a significant class of cyber threats that modify PSSE by maliciously altering the measurement data. In FDIAs, an attacker changes sensor data in such a way that a valid and misleading operating point converge in PSSE and the attack becomes unobservable [6]. Being unaware of the malicious data, the grid operator takes actions according to the false operating point of grid and consequently disrupts power system operation.

Traditional PSSE is performed using the weighted least squares estimation (WLSE) technique, and the presence of bad data is detected by employing the largest normalized residual test (LNRT) [4]. Stealth (unobservable) FDIA can easily bypass the bad data detection (BDD) systems. Therefore, FDIAs are one of the most critical attacks for today's smart

power systems. FDIs in power grids were first introduced a decade ago by [7], which showed that an attacker with enough knowledge of the grid topology can design an unobservable attack that satisfies the power flow equations and bypasses the BDD module. Influential reference [7] prompted an increased interest in detection of FDIs [8], [9], [10], [11], [12], [13], [14], [15], [16], [17], [18], [19], [20], [21].

Most of the works that deal with detection of FDIs assume a linearized DC model [7], [8], [9], [10], [12], [14], [15], [17], [20]. In the DC state estimation model, bus voltage magnitudes are assumed to be known as 1 p.u. and branch resistances and shunt elements are neglected. Hence, estimation of bus voltage angles is reduced to linear matrix operations, and in general it helps to analyze the grid at some extent. Although the linearized DC model is fast and simple, ignoring voltage magnitudes and reactive power components does not reflect the actual physical operation of the grid [4]. Therefore, the DC models can not validate that the FDIs being tested are stealthy because PSSE and BDD tools employing AC power flow modeling can easily detect these attacks without using extra detectors. In addition, only a few works exploit grid topology information into their detection model [22], [11], [23] together with graph signal processing (GSP) techniques to detect FDIs. Although innovative and powerful, these methods manually design spectral filters, an operation which is not scalable since it requires manual and custom filter design steps. Scalability is an essential feature that has to be considered when designing detectors. Except a few highly scalable designs [24], [25], the majority of the proposed detectors for FDIs are designed for small scale systems such as IEEE 14 [12], [14], [15], [16] or IEEE 30 [18], [20]. Therefore, extensibility issues may arise when deploying small-scale detectors at large-scale networks. Employing spatial-temporal correlations of the state variables and trust-based voting mechanisms, reference [8] defines a consistency region and detection threshold to differentiate honest from malicious samples. Nevertheless, DC approximation and resolution of the time series data highly limit the applicability of the proposed design to realistic large-scale power grids.

Survey [26] classifies the FDIA detection algorithms into two categories: model-based methods [12], [13], [14], [15], [16] and data-driven methods [17], [18], [19], [20], [21]. In general, model-based algorithms require first to build a system model and estimate its parameters to detect FDIs. Since there is no independent system to be trained, model-based methods do not need historical datasets; nevertheless, threshold finding, detection delays and scalability aspects restrict applicability of model-based methods [26]. On the contrary, data-driven models do not interfere with the system and its parameters, yet they necessitate historical data and a training process in order to reduce the detection time and increase scalability.

Due to the superiority of machine learning (ML) methods along with the increasing volume of collected historical data samples, ML-based detectors have been proposed to identify FDIs in smart grids. For example, Decision Tree (DT) [21], Support Vector Machine (SVM) [17], [18] Multi Layer Perceptron (MLP) [18], Recurrent Neural Network (RNN) [20], Convolutional Neural Network (CNN) [19] models were

proposed to detect FDIs. Despite their effectiveness, ML-based methods may overfit and fail to detect FDIs especially in situations when the ML architecture does not capture the underlying physical system generating the data [26]. To illustrate, CNNs are well-suited to image and video processing since locality of pixels is well modeled by the sliding kernels. Conversely, an RNN architecture might be more applicable to recurrent relations such as sequence to sequence language modeling and machine translation applications [27].

Undirected graphs can be used to capture the smart grid topology; buses and branches of the grid can be represented by nodes and edges of the undirected graph, respectively. The Graph Neural Network (GNN) architecture, in particular, immensely benefits from this architectural matching promise. Besides, the prediction of the filter weights in GNNs instead of being performed manually (e.g., [22], [11], [23]) can be executed automatically via GSP techniques which makes GNNs more attractive to smart grid applications. Therefore, GNNs where proposed for optimal power flow applications in power grids [28]. Despite their potential, to the best of our knowledge, no study has explored GNNs to detect FDIs.

In this paper, we propose a GNN-based stealth FDIA detection model for smart power grids. To fully model the underlying complex AC power system and dynamism of the measurements data, we decided to use a hybrid model; while system topology is integrated into our model by the help of GNN graph adjacency matrix, historical measurement data are modeled by the GNN spatial layers. These features enable to take advantage of the benefits of both model-driven and data-driven approaches and hence better detect and mitigate FDIs.

The contributions of this paper are summarized as follows:

- We accurately model the underlying physical system: linearized DC models are crude approximations of actual AC power systems and inaccurate to model smart grids. Thus, the AC power flow equations are considered for more accurate modeling.
- We properly model the inherent cyber system: due to the topology and distribution of the smart measurement devices, meter readings are correlated in the measurement space of the smart grid; hence, ignoring the location of the meter data and assuming independent and identical distribution (iid) of meter readings may not be accurate for a data-driven model. Therefore, we use GNN to match the cyber and physical layers of the grid.
- We design a stealth FDIA attack methodology to test our detector. The main goal of any FDIA detector is to be able to detect stealth attacks since observable attacks can be easily detected by BDD systems. In other words, unproven random attacks do not require any extra detector other than traditional BDDs so the proposed detectors should be tested under stealth attacks to fully evaluate their performances. Therefore, we develop a Stochastic Gradient Descent (SGD) based stealth FDIA detection algorithm to exploit the possible weak points of the grid and assess the performance in realistic conditions. It is experimentally verified that the designed attacks can easily bypass classical BDD algorithms; however, they are detected by the proposed GNN detectors.

- We propose a scalable and real-time solution: custom methods developed for small case systems may not be applicable to larger cases; therefore, detection models should be efficiently extensible to larger networks. Moreover, depending on the system scale and topology, detection delays can be very critical for power grids, therefore possible attacks should be detected as quick as possible. Employing the standard test cases such as IEEE 14, 118, and 300 bus systems, it is demonstrated that the proposed method is linearly scalable both in parameter size and detection time.

The remainder of this paper is divided into five sections. Section II is devoted to preliminaries such as power system state estimation, false data injection attacks and bad data detection mechanism in smart grids. While Section III explains the proposed detection method and its mathematical modeling, Section IV describes the experimental results. Finally, Section V concludes the paper.

## II. POWER SYSTEM PRELIMINARIES

Herein section, a short overview of power system basics is presented to facilitate description of proposed algorithms.

### A. Power System State Estimation

PSSE module aims to estimate the system state  $\mathbf{x}$  ( $V_i, \theta_i$  at each bus) in the steady state by using the complex power measurements  $\mathbf{z}$  collected by noisy RTUs or PMUs via:

$$\hat{\mathbf{x}} = \min_{\mathbf{x}} (\mathbf{z} - h(\mathbf{x}))^T \mathbf{R}^{-1} (\mathbf{z} - h(\mathbf{x})), \quad (1)$$

where  $\mathbf{R}$  denotes the error covariance matrix of measurements and  $\mathbf{z}$  consists of active and reactive powers injections at buses ( $P_i, Q_i$ ) and active and reactive power flows on branches ( $P_{ij}, Q_{ij}$ ). In polar form, these can be expressed as [4]:

$$\begin{aligned} P_i &= \sum_{j \in \Omega_i} V_i V_j (G_{ij} \cos \theta_{ij} + B_{ij} \sin \theta_{ij}) = P_{Gi} - P_{Li} \\ Q_i &= \sum_{j \in \Omega_i} V_i V_j (G_{ij} \sin \theta_{ij} - B_{ij} \cos \theta_{ij}) = Q_{Gi} - Q_{Li} \\ P_{ij} &= V_i^2 (g_{si} + g_{ij}) - V_i V_j (g_{ij} \cos \theta_{ij} + b_{ij} \sin \theta_{ij}) \\ Q_{ij} &= -V_i^2 (b_{si} + b_{ij}) - V_i V_j (g_{ij} \sin \theta_{ij} - b_{ij} \cos \theta_{ij}). \end{aligned} \quad (2)$$

Since (2) are nonlinear and non-convex, minimization in (1) is carried out via iterative weighted least squares estimation (WLSE) [29].

### B. False Data Injection Attacks

The goal of FDIA is to find a new measurement vector  $\mathbf{z}_a$  in the measurement space of the grid such that PSSE converges to another point in the state space of variables. Formally,

$$\begin{aligned} \mathbf{z}_o &= h(\hat{\mathbf{x}}) \\ \mathbf{z}_a &= \mathbf{a} + \mathbf{z}_o = h(\hat{\mathbf{x}}), \end{aligned} \quad (3)$$

where  $\mathbf{a}$  represents the attack vector,  $\hat{\mathbf{x}}$  and  $\hat{\mathbf{x}}$  denote the estimated (original) state vector and false data injected state vector, and  $\mathbf{z}_o$  and  $\mathbf{z}_a$  stand for the original and attacked measurements, respectively.

### C. Bad Data Detection

Traditional power systems use the largest normalized residual test (LNRT) to detect bad samples using below eqs. [4]:

$$\begin{aligned} \mathbf{r} &= \mathbf{z} - h(\hat{\mathbf{x}}) \\ \mathbf{G} &= \mathbf{H}^T \mathbf{R}^{-1} \mathbf{H} \\ \mathbf{S} &= \mathbf{I} - \mathbf{H} (\mathbf{G}^{-1} \mathbf{H}^T \mathbf{R}^{-1}) \\ \mathbf{r}_i^N &= \frac{|\mathbf{z}_i - h(\hat{\mathbf{x}})_i|}{\mathbf{R}_{ii} \mathbf{S}_{ii}}. \end{aligned} \quad (4)$$

After estimating the current state vector using eq. (1), residues  $\mathbf{r}$  are calculated as the difference between observed ( $\mathbf{z}$ ) and calculated ( $h(\hat{\mathbf{x}})$ ) measurements. Then, using Jacobian matrix  $\mathbf{H}$  and diagonal error covariance matrix of the measurements  $\mathbf{R}$ , gain matrix  $\mathbf{G}$  is computed. Sensitivity of the residues for each measurement represented by the residual sensitivity matrix  $\mathbf{S}$  are computed right after  $\mathbf{G}$ . Finally, residues are normalized by dividing each one of them with the product of corresponding diagonal elements of  $\mathbf{R}$  and  $\mathbf{S}$ , and normalized residue vector  $\mathbf{r}^N$  is obtained. Since  $\mathbf{r}^N$  is assumed to have a standard normal distribution, a large  $r_i^N$  can be classified as bad data, if  $r_i^N$  exceeds a predetermined threshold  $\tau_{bdd}$  specified by the grid operator according to the desired level of sensitivity [4]. If an attacker wants to be considered stealthy, the maximum normalized residual value  $\max(\mathbf{r}^N)$  should be less than the threshold  $\tau_{bdd}$ .

## III. GNN BASED DETECTION OF FDIA

After introducing the power system operation preliminaries, we formulate the proposed GNN detector herein section.

### A. False data injection attack scenario

The main architecture and signal flow of the proposed design is illustrated in Fig. 1. First, active and reactive power injections  $P_i, Q_i$  at buses and active and reactive power flows  $P_{ij}, Q_{ij}$  on branches are read by RTUs. Next, as a man in the middle, an attacker attempts to inject false data to the original measurements  $\mathbf{z}_o = [P_i, P_{ij}, Q_i, Q_{ij}]$  before the grid operator receives them. Then, using  $\mathbf{z}_a$ , the operator estimates the state variables and runs the BDD block to indicate a possible attack. In parallel, the defender runs the GNN-based detector when it receives the measurements and hence predicts the probability of attack to warn the operator. In order not to raise suspicion from the operator, the attacker needs to design a stealth  $\mathbf{z}_a$  that can bypass the BDD mechanism incorporated in eq. (4). At the same time, the attack strength should be strong enough to cause intended consequences or damages to the grid. In this regard, s/he initially estimates the state variables of grid in the target area  $\mathcal{T}$ , where security of the meters is compromised. Then, s/he searches a set of measurements  $\mathbf{z}_a$  in the measurement space that serves the intended aim.

As indicated by [1], [7], FDIA require that an adversary know the parameters and topology of the targeted portion of system and is able to tamper the measurement data before the operator uses them in PSSE. Since accessing information and hardware all over the grid is neither easy nor realistic, we use a realistic ‘local’ attack model to test our system.

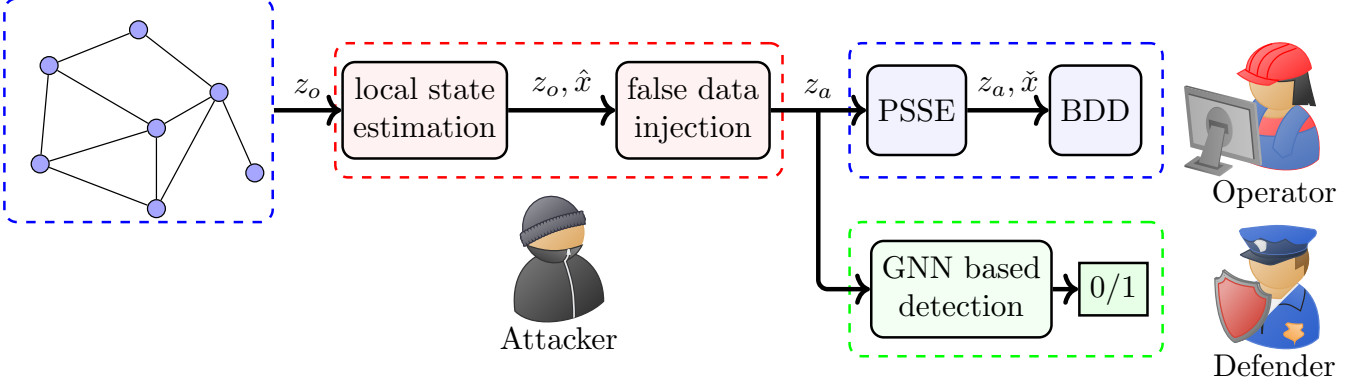


Fig. 1. Architectural overview and signal flow graph of the proposed design. While blue boxes represent smart grids and their operations run by operator, red and green boxes denote functional blocks of attacker and defender, respectively. Note that operator gets attacked measurements  $z_a$  instead of original ones  $z_o$  due to the FDIA. Defender, on the contrary, tries to detect possible attacks by using  $z_a$ .

Due to the lack of open source, AC power flow based stealth FDIA generation algorithms to fully test the detection system, we propose a generic, localized AC stealth FDIA generation method using the stochastic gradient descent algorithm. Herein scenario, the attacker focuses on a target area of the grid where the measurements s/he wants to inject the false data are located. To specify this area, it is assumed that s/he found an entry point  $p$  in the cyber layer and can manipulate the measurements up to the  $r$ -neighbor of  $p$ . Since generation buses and zero-injection buses would be too risky to change, s/he skips those buses even if they are in their active target region. An example IEEE 14 case system is demonstrated in Fig. 2, where an attacker's entry point  $p$  is bus 10 and his radius  $r$  is 2, so s/he can change the measurements of buses 10 (entry point), 9 and 11 (1-degree neighbors), and 4, 7, 6, 14 (2-degree neighbors) designated with red stars. Note that s/he skips bus 6 since it is a generator node designated by a green square. In addition, it is presumed that s/he can alter the measurements of the power flows in the active area represented by red dashed lines. All the other measurements outside the target region  $\mathcal{T}$  represented by red surface are presumed to be still secure to the attacker.

To find a stealth attack vector in  $\mathcal{T}$ , the attacker tries to minimize the objective function:

$$\begin{aligned} \min_{\tilde{x}} \lambda_z \|h(\tilde{x})_i - h(\hat{x})_i\|_2 - \lambda_x \|\tilde{x}_j - \hat{x}_j\|, \forall i \in \mathcal{T}_z, \forall j \in \mathcal{T}_x \\ \text{s.t. } h(\tilde{x})_k = h(\hat{x})_k, \tilde{x}_l = \hat{x}_l, \forall k \notin \mathcal{T}_z, \forall l \notin \mathcal{T}_x \\ \tau_m^{\min} < \|\tilde{x}\| < \tau_m^{\max}, \tau_a^{\min} < \angle(\tilde{x}) < \tau_a^{\max}, \end{aligned} \quad (5)$$

where  $\hat{x}$  denotes the honest state vector,  $\tilde{x}$  stands for false data injected state vector,  $\lambda_z$  and  $\lambda_x$  are weighting factors associated with loss terms,  $\mathcal{T}_z$  and  $\mathcal{T}_x$  denote the targeted measurements and state variables,  $\tau_m^{\min}$  and  $\tau_m^{\max}$  denote the minimum and maximum values of the magnitude of  $\tilde{x}$ , and  $\tau_a^{\min}$  and  $\tau_a^{\max}$  represent minimum and maximum values of the angle of  $\tilde{x}$ , respectively. In essence, s/he searches a vector  $\tilde{x}$  in the state space of the grid  $\mathfrak{X}$  by only targeting some  $x \in \mathcal{T}_x$  so that the corresponding measurements  $z_a = h(\tilde{x})$  resemble the original measurements  $z_o$  in the measurement space of the grid  $\mathfrak{Z}$  restricted by  $\mathcal{T}_z$ . Note that the objective

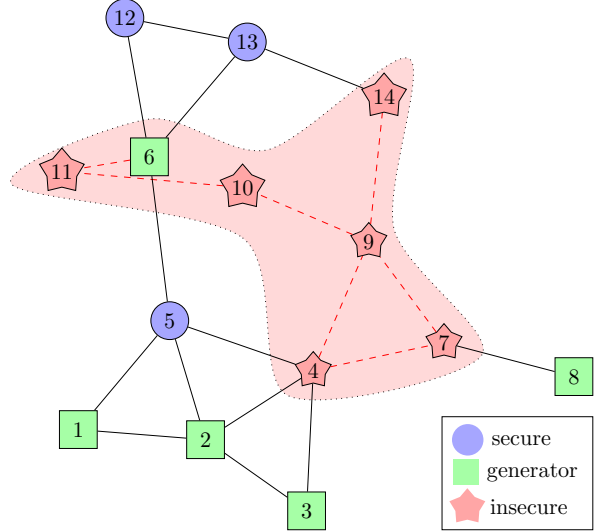


Fig. 2. Visualization of an example IEEE 14 bus system where an attacker enters the system from bus 10 (entry point) and affects the 1-degree neighbors: bus 9 and 11, and 2-degree neighbors: bus 4, 7, 6, 14 depicted with red stars. Besides, it is assumed that s/he can change the power flows measurements depicted with red dashed lines in the target area  $\mathcal{T}$  represented by the red surface. Note that since bus 6 is a generator node illustrated by a green square s/he skips it.

function in (5) consists of two competing losses. While the first part  $\|h(\tilde{x})_i - h(\hat{x})_i\|_2$  aims to minimize the measurement differences in  $\mathcal{T}_z$ , the second part  $\|\tilde{x}_j - \hat{x}_j\|$  maximizes the attack power injected into the state variables in  $\mathcal{T}_x$ . The trade-off between these objectives is directly related to detection risk and attack power since deviation from the original state variables increases the probability of being detected. Consequently, an attacker can increase the attack power at the expense of higher risk of being detected.

An obvious and natural solution to this minimization problem would be  $\tilde{x}_j = \hat{x}_j$ , which means no attack at all, and a smart attacker avoids this trivial solution. Instead, the attacker aims to maximize the assault power by minimizing

the detection risk. To do that, s/he first defines a free complex variable  $\tilde{x}_j \in \mathfrak{X}$  in the vicinity of original estimated values by probing them with a small Gaussian noise. Then, by the help of SGD algorithm, s/he calculates the gradient of the state variables with respect to the joint loss defined in (5) and updates them iteratively at each step until there is no improvement in the loss. Recall that s/he only updates a state variable if it is in the active insecure area. Eventually, s/he decides whether to inject this obtained false data to the related measurements in the cyber layer of the grid, according to the final loss value obtained during the iterations. In a sense, this individual latent vector search can be interpreted as ‘training’ in the machine learning terminology [30]; however, it is very specific to the corresponding time slot and should be repeated for each case in order to minimize the detection risks. Note that this generic algorithm can be tailored according to the modeled electric grid and capabilities of the attacker.

### B. Graph Neural Network modeling of Smart Grids

Smart power grids can be modeled by a connected, undirected, weighted graph  $\mathcal{G} = (\mathcal{V}, \mathcal{E}, \mathbf{W})$  that consists of a finite set of vertices  $\mathcal{V}$  with  $|\mathcal{V}| = n$ , a finite set of edges  $\mathcal{E}$  and a weighted adjacency matrix  $\mathbf{W} \in \mathbb{R}^{n \times n}$  [31]. Buses are represented by vertices  $\mathcal{V}$ , branches and transformers are represented by edges  $\mathcal{E}$  and line admittances are represented by  $\mathbf{W}$  in this mapping. If the buses  $i$  and  $j$  are connected, the corresponding weight of the edge  $e = (i, j)$  connecting vertices  $i$  and  $j$  is assigned to  $W_{ij}$ . A signal or a function  $f : \mathcal{V} \rightarrow \mathbb{R}$  in  $\mathcal{G}$  can be represented by a vector  $\mathbf{f} \in \mathbb{R}^n$ , where  $i$ th component of the vector  $\mathbf{f}$  corresponds to scalar value at the vertex  $i \in \mathcal{V}$ .

A fundamental operator defined in spectral graph theory [32] is the graph Laplacian operator  $L \in \mathbb{R}^{n \times n}$ . Its normalized definition is represented as:

$$L = I_n - D^{-1/2} \mathbf{W} D^{-1/2}, \quad (6)$$

where  $I_n$  is the identity matrix, and  $D \in \mathbb{R}^{n \times n}$  is the diagonal degree matrix with  $D_{ii} = \sum_j W_{ij}$ . Since  $L$  is a real symmetric positive semi-definite matrix, all eigenvalues  $\lambda_i$  of it are real valued and non-negative, and it has complete set of orthonormal eigenvectors  $\mathbf{u}_i$  [31]. Thus,  $L$  can be diagonalized:

$$L = U \Lambda U^T, \quad (7)$$

where  $U = [\mathbf{u}_0, \mathbf{u}_1, \dots, \mathbf{u}_{n-1}] \in \mathbb{R}^{n \times n}$  represent the  $n$  orthonormal eigenvectors, and  $\Lambda = \text{diag}([\lambda_0, \lambda_1, \dots, \lambda_{n-1}]) \in \mathbb{R}^{n \times n}$  denotes the diagonal matrix of  $n$  eigenvalues  $0 = \lambda_0 < \lambda_1 < \dots < \lambda_{n-1} < 2$  due to the normalization [31]. In fact, vectors  $\mathbf{u}_i$  form the graph Fourier basis and  $\lambda_i$  values represent frequencies in graph spectral domain [33].

After representing the Fourier basis and frequencies, the Fourier Transform and its inverse can be defined in the graph spectral domain analogously to the classical Fourier Transform. Namely, the Graph Fourier Transform (GFT) and Inverse Graph Fourier Transformation (IGFT) are defined as:

$$\begin{aligned} \tilde{s} &= U^T s & (\text{GFT}) \\ s &= U \tilde{s} & (\text{IGFT}) \end{aligned}$$

where  $s$  and  $\tilde{s}$  denote vertex and spectral domain signals, respectively.

Unlike classical signal processing, a meaningful translation operator does not exist in the vertex domain [34]. Therefore, to apply a convolution operation to graph signals, they are first transformed into the spectral domain using GFT, then convolved (Hadamard product) in the spectral domain and finally the result transformed back to the vertex domain using IGFT [34]. Formally,

$$x *_{\mathcal{G}} y = U((U^T x) \odot (U^T y)) \quad (8)$$

Similarly, a graph signal  $x \in \mathbb{R}^n$  is filtered by a kernel  $g_\theta$ :

$$y = g_\theta *_{\mathcal{G}} x = g_\theta(U \Lambda U^T)x = U g_\theta(\Lambda) U^T x \in \mathbb{R}^n, \quad (9)$$

where  $g_\theta(\Lambda) = \text{diag}(\theta)$  is a non-parametric kernel, and  $\theta \in \mathbb{R}^n$  is a vector of Fourier coefficients [33]. To put it differently,  $g_\theta$  filters the signal  $x$  in the spectral domain by multiplying its spectral components with the free  $\theta$  coefficients in a similar way with the classical signal processing in the Fourier domain. Eventually, the filtered signal is transformed back to the vertex domain by IGFT [33]. Nevertheless, those non-parametric filters are not spatially localized and hence computational complexity of eq. (9) is  $\mathcal{O}(n^2)$  due to the matrix multiplication with  $U$ . To thwart this problem, [34] proposed to parameterize  $g_\theta(L)$  as a Chebyshev polynomial function which can be computed recursively from  $L$ .

The  $K$  order Chebyshev polynomial of the first kind  $T_k(x)$  is computed recursively as follows [35]:

$$T_k(x) = \begin{cases} 1 & k = 0 \\ x & k = 1 \\ 2xT_{k-1}(x) - T_{k-2}(x) & k \geq 2. \end{cases} \quad (10)$$

Therefore, a filter  $g_\theta$  can be approximated by a truncated expansion of Chebyshev polynomials,  $T_k$ , up to order  $K - 1$  and a signal  $x$  can be filtered by  $g_\theta$ :

$$y = g_\theta *_{\mathcal{G}} x = g_\theta(L)x = \sum_{k=0}^{K-1} \theta_k T_k(\tilde{L})x, \quad (11)$$

where the parameter  $\theta \in \mathbb{R}^K$  is a vector of Chebyshev coefficients, and  $T_k(\tilde{L}) \in \mathbb{R}^{n \times n}$  is the Chebyshev polynomial of order  $k$  evaluated at the scaled Laplacian  $\tilde{L}$  given by:

$$\tilde{L} = 2L/\lambda_{max} - I_n. \quad (12)$$

Finally, filtered signal  $y$  can be calculated by the help of (10) and (11) as:

$$y = \sum_{k=0}^{K-1} \theta_k \bar{x}_k, \quad (13)$$

where  $\bar{x}_k$  is computed recursively:

$$\bar{x}_k = \begin{cases} x & k = 0 \\ \tilde{L}x & k = 1 \\ 2\tilde{L}\bar{x}_{k-1} - \bar{x}_{k-2} & k \geq 2. \end{cases} \quad (14)$$

Note that convolution in eq. (13) is  $K$ -localized, and its computational complexity is reduced to  $\mathcal{O}(K|\mathcal{E}|)$ . For detailed analysis, please refer to [34], [33], [31].

### C. Detection of attacks using Graph Neural Network

The architecture of the proposed GNN-based detector is depicted in Fig. 3. It contains one input layer to represent bus power injection measurements,  $L$  hidden Chebyshev graph convolution layers to extract spatial features and one output dense layer to predict the probability of the input sample being attacked. In this layered structure,  $X^0$  denotes two channel input tensor  $[P_i, Q_i] \in \mathbb{R}^{n \times 2}$ ,  $X^l$  represents the output tensor of hidden layer  $l \in \mathbb{R}^{n \times c_l}$ ,  $y \in \mathbb{R}$  designates the scalar output of the neural network,  $1 \leq l \leq L$ , and  $c_l$  stands for the number of channels in layer  $l$ . Particularly, a GNN hidden layer  $l$  takes  $X^{l-1} \in \mathbb{R}^{n \times c_{l-1}}$  as input and produces  $X^l \in \mathbb{R}^{n \times c_l}$  as output. Different from the hidden graph layers, dense layer outputs  $y$  in classical feed-forward neural networks by feeding with the inputs  $X^L \in \mathbb{R}^{n \times c_L}$ . In this multi-layer architecture,

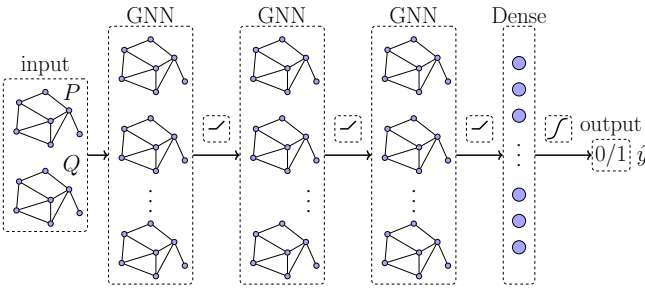


Fig. 3. Architecture of the proposed GNN based detector.

each Chebyshev layer  $l$  for  $1 \leq l \leq L$  transforms its input  $X^{l-1}$  by first applying graph convolution operation using eqs. (13) and (14), then adding a bias term and finally employing a nonlinear rectified linear unit function (ReLU) defined as  $\text{ReLU}(x) = \max(0, x)$  to generate  $X^l$ . Namely,

$$X^l = \text{ReLU}(\theta^l * g X^{l-1} + b^l), \quad (15)$$

where  $\theta^l \in \mathbb{R}^{K \times c_{l-1} \times c_l}$  denotes free Chebyshev coefficients and  $b^l \in \mathbb{R}^{c_l}$  represents bias term of the layer  $l$ . Recall that each Chebyshev layer gets extra scaled Laplacian  $\tilde{L}$  values calculated by eq. (12). In a similar fashion, output of the dense layer is computed by  $y = \sigma(W^L X^L + b^L)$ , where  $W^L \in \mathbb{R}^{n \times c_L}$  denotes the weights of each feature,  $b^L \in \mathbb{R}$  represents the bias term and  $\sigma$  designates the nonlinear sigmoid operation:  $\sigma(x) = 1/(1 + e^{-x})$ .

## IV. EXPERIMENTAL RESULTS

### A. Data Generation

Generating reliable data is the first step in building a successful defense mechanism since all the future blocks depend on it. Since it is not possible to find publicly available power grid data due to the privacy issues, synthetic data are generated using Pandapower [36] for several test cases including IEEE 14, 118, and 300. Data generation steps are summarized in Algorithm 1. To make the data as realistic as possible, we first downloaded ERCOT's 15 minutes interval backcasted actual load profiles [37]. Next, we arbitrarily selected 'BUSHILF\_SCENT' profile which corresponds to south-central of Texas having high load factor. Then, we

### Algorithm 1: Data generation

---

```

Input : normalized scaler  $S$  //  $\mu = 0$ ,  $\sigma = 1$ 
Output:  $Z_n, X_n$  for each test system  $n$ 
1  $N \leftarrow [14, 118, 300]$  // IEEE bus systems
2  $T \leftarrow [1 \text{ to } 5000]$  // timestep index
3  $k, \sigma_s \leftarrow 0.1, 0.03$  // scaling coefficients
4  $\sigma_n \leftarrow 0.01$  // noise coefficient
5 Function Generate( $sg, t$ ):
6   foreach bus  $\in sg.genbus \cup sg.loadbus$  do
7      $bus.scale \leftarrow \mathcal{N}(1 + k \cdot S_t, \sigma_s^2)$ 
8      $z_o = sg.PF()$  // run AC power flow
9      $z_o \leftarrow \mathcal{N}(z_o, z_o \cdot \sigma_n^2)$ , // 1% additive noise
10     $\hat{x} \leftarrow sg.PSSE(z_o)$  // estimate state
11    return  $z_o, \hat{x}$ 
12 Function Main:
13   foreach  $n \in N$  do
14      $Z_n, X_n \leftarrow [], []$  // empty vectors
15      $sg \leftarrow SG(n)$  // smart grid obj.
16     foreach  $t \in T$  do
17        $z, x \leftarrow \text{Generate}(sg, t)$ 
18        $Z_n[t], X_n[t] \leftarrow z, x$  // append
19    $Z_n.save(), X_n.save()$ 

```

---

normalized the time series data to zero mean and unit variance 'scaler' vector  $S$  so that it can be easily adapted to each test system. Having obtained  $S$ , we run the Main function of the Algorithm 1 where a smart grid object  $sg$  is created for each test system having  $n$  bus and Generate function is called for each timesteps  $t$ . In Generate function, the scaling parameters of generator and load buses are assigned to a sample drawn from a normal distribution with  $1 + 0.1 \cdot S_t$  mean and  $0.03^2$  variance, where  $S_t$  denotes the value of  $S$  at time-step  $t$ . Due to the properties of normal distribution, the scaling operation provides practically more than  $\pm 20\%$  dynamic range in average with respect to the static case. As a next step, AC power flow solutions are calculated, and the measurements considered to have 1% noise are read. Finally, PSSE is conducted, and estimated state variables are returned along with original meters values to the Main function.

### B. Attack Generation

After generating honest data samples, we focus on malicious data samples in this subsection, where the attack generation steps are summarized in Algorithm 2. The algorithm gets original measurements matrix  $Z_n \in \mathbb{R}^{T \times m}$  and estimated state variable matrix  $X_n \in \mathbb{R}^{T \times n}$  and produces their attacked version as well as corresponding sample vector  $Y_n \in \mathbb{R}^T$ , where 0 and 1 in  $Y_n$  represent honest and malicious samples, respectively. As can be seen from Algorithm 2, Main function simply creates the smart grid and attacker objects, fetches the current sample and calls Generate function for each system having  $n$  buses at each time-step  $t$ .

Generate function, in contrast, simulates a 'smart' intruder capable of entering the cyber layer of the grid, computing an

unobservable attack vector and deciding to insert the false data into the measurement devices according to the ‘quality’ of the attack. In this regard, since it is not realistic to assume that an attacker can inject false data at every time step due to practical reasons, Generate function first models the attack frequency by a r.v.  $f \sim \mathcal{N}(0, 1)$  where  $f > \tau_{freq}$  means the attacker has successfully entered the system. To attack roughly 15% of total time-steps on average,  $\tau_{freq}$  is selected as 1. Second, it models the target area of the attacker  $\mathcal{T}$  similar to the red area given with Fig. 2 by help of a r.v.  $p \sim \mathcal{U}(1, n)$  and a predefined attack radius  $r$ . To this end, it calls a breadth first search (BFS) method of the attacker object to model the target area defined by a set of measurements captured by the attacker denoted by  $\mathcal{T}_z$  and a set of state variables  $\mathcal{T}$  intended to inject the false data. In fact, all the measurements and state variables located up to  $r$ -distance neighbor of the bus  $p$  are assumed to be in  $\mathcal{T}_z$  and  $\mathcal{T}_x$  except the generator buses and zero-injection buses. Then, it calls the attack method of the attacker to compute and insert  $z_a$  if the method returns a *loss* value smaller than threshold  $\tau_{loss}$ .

The attacker’s assault method solves the nonlinear and non-convex minimization (5) in the Tensorflow [38] library. As a first step, it defines a free trainable vector tuple to represent the new complex state variables  $\check{x}$  which constitutes the ‘fake’ operating point at the end of attack: voltage magnitude  $\mathbf{V}$  is limited to  $0.9 < \mathbf{V} < 1.1$  p.u. and voltage angle  $\theta$  is limited to  $-\pi < \theta < \pi$ . Next, it initializes the  $j$ th elements of this tuple in the vicinity of their original variables by adding a small Gaussian white noise  $\mathcal{N}(0, \sigma_n^2)$  if  $j \in \mathcal{T}_x$  to ignite the optimization. This small proximity could play a vital role because SGD may fail to reduce the objective function if the initial point is not balanced [30]. A  $\check{x}$  too close to  $\hat{x}$  might result to no update at all in optimization variables  $\mathbf{V}$  and  $\theta$ , whereas a  $\check{x}$  too distant to  $\hat{x}$  might get stuck in a secluded region of  $\mathfrak{X}$  and produce a highly suspicious  $z_a$ . Thus,  $\sigma_n = 0.005$  is found to be accurate according to the minimization loss. Then, for each epoch, it obtains  $z_a$  using  $h(\mathbf{x})$  and consequently calculates loss term  $L_z$  as a root mean squared error between  $z_a$  and  $z_o$ , and  $L_x$  as a mean absolute error between  $\check{x}$  and  $\hat{x}$ . Eventually, it calculates gradients of total loss  $L = \lambda_z L_z - \lambda_x L_x$  with respect to optimization variables  $\mathbf{V}_j$  and  $\theta_j \in \mathcal{T}_x$  and updates corresponding terms in the reverse direction of gradients by scaling the gradients with learning rate  $\eta$  before starting the next epoch. Lastly, it returns  $z_a$  and final loss  $L$  to Generate function and halts. Distributions of some important values of IEEE 300 test system are given in Fig. 4 after running Algorithm 2.

### C. Attack Detection

In order to immediately predict the attack probability in our models instead of waiting for PSSE result, we only use measurement values in our detectors. Moreover, since  $P_i + jQ_i = \sum_{k \in \Omega_i} P_{ik} + jQ_{ik}$ , node values can represent branch values as summation in their corresponding  $\Omega_i$  and the proposed GNN-based detector accepts features in its nodes, we decide to use only  $P_i$  and  $Q_i$  as input to our models. PSSE and BDD modules, on the contrary, continue to receive every available measurement to operate as depicted in Fig. 1.

---

### Algorithm 2: Attack generation

---

```

Input :  $Z_n, X_n$  for each test system  $n$ 
Output:  $Z_n, X_n, Y_n$  for each test system  $n$ 
1  $N \leftarrow [14, 118, 300]$  // IEEE bus systems
2  $T \leftarrow [1 \text{ to } 5000]$  // timestep index
3  $\sigma_n \leftarrow 0.005$  // initial disturbance
4  $\lambda_z, \lambda_x \leftarrow 1, 1$  // loss weights
5  $\eta, E \leftarrow 0.001, 1000$  // learning rate and epochs
6  $\tau_{freq}, \tau_{loss} \leftarrow 1, 0.1$  // attackers thresholds
7  $R \leftarrow \{14 : 2, 118 : 8, 300 : 10\}$  // radius dict.

Function attacker.attack( $z_o, \hat{x}, \mathcal{T}_z, \mathcal{T}_x$ ):
9    $trainable \mathbf{V} : 0.9 < \mathbf{V} < 1.1$ 
10   $trainable \theta : -\pi < \theta < +\pi$ 
11   $V, \theta \leftarrow \text{abs}(\hat{x}), \text{angle}(\hat{x})$ 
12  foreach  $j \in \mathcal{T}_x$  do
13     $V_j \leftarrow V_j + \mathcal{N}(0, \sigma_n^2)$ 
14     $\theta_j \leftarrow \theta_j + \mathcal{N}(0, \sigma_n^2)$ 
15  foreach  $epoch \in E$  do
16     $\check{x} \leftarrow V e^{j\theta}$  // complex state vars.
17     $z_a \leftarrow h(\check{x})$  // real measurements
18     $L_z \leftarrow \sum_i \|z_{ai} - z_{oi}\|_2, \forall i \notin \mathcal{T}_z$ 
19     $L_x \leftarrow \sum_j \|\check{x}_j - \hat{x}_j\|, \forall j \notin \mathcal{T}_x$ 
20     $L \leftarrow \lambda_z L_z - \lambda_x L_x$ 
21    foreach  $j \in \mathcal{T}_x$  do
22       $V_j \leftarrow V_j - \eta \frac{\partial L}{\partial V_j}$ 
23       $\theta_j \leftarrow \theta_j - \eta \frac{\partial L}{\partial \theta_j}$ 
24     $\check{x} \leftarrow V e^{j\theta}$  // complex state vars.
25     $z_a \leftarrow h(\check{x})$  // real measurements
26  return  $z_a, L$ 

27 Function Generate(attacker,  $z_o, \hat{x}$ ):
28   $y, z \leftarrow 0, z_o$  // no attack yet
29   $f \sim \mathcal{N}(0, 1)$  // attack frequency
30  if  $f > \tau_{freq}$  then
31     $p \sim \mathcal{U}(1, n)$  // entry point
32     $r \leftarrow R[n]$  // attack radius
33    /* determine attack surface by BFS */
34     $\mathcal{T}_z, \mathcal{T}_x \leftarrow \text{attacker.BFS}(p, r)$ 
35     $z_a, loss \leftarrow \text{attacker.attack}(z_o, \hat{x}, \mathcal{T}_z, \mathcal{T}_x)$ 
36  if  $loss < \tau_{loss}$  then
37     $y, z \leftarrow 1, z_a$  // attack injected
38   $\check{x} \leftarrow sg.PSSE(z)$ 
39  return  $z, \check{x}, y$ 

38 Function Main:
39  foreach  $n \in N$  do
40     $Y_n \leftarrow []$  // empty label vector
41     $sg \leftarrow \text{SG}(n)$  // smart grid obj.
42     $attacker \leftarrow \text{Attacker}(n)$  // attacker obj.
43    foreach  $t \in T$  do
44       $Z_n[t], X_n[t], Y_n[t] \leftarrow$ 
45       $\text{Generate}(attacker, Z_n[t], X_n[t])$ 
46       $X_n.save(), Z_n.save(), Y_n.save()$ 

```

---

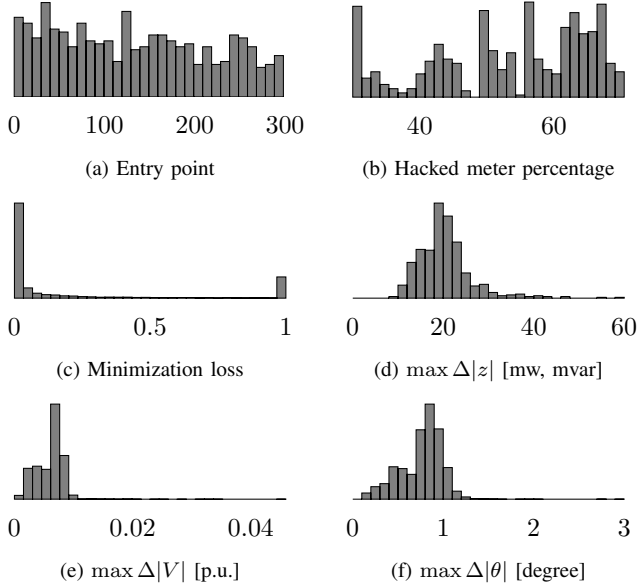


Fig. 4. Distributions of attacker's entry point (4a), ratio of seized meters in percentage (4b), minimization loss values by solving eq. (5) (4c), maximum absolute difference of attack to measurements and maximum absolute difference of state variables due to attacks in terms of voltage magnitude (4e) and angle (4f) obtained by Algorithm 2. Roughly speaking, the attacker initiates the assault arbitrarily and uniformly from any node (Fig. 4a) by capturing 50% of the available meters on average (Fig. 4b) and succeeding 73.7% of the attempts (Fig. 4c). Adding maximum 20 mw or 20 mvar of attack to measurement devices (Fig. 4d) creates maximum 1% deviation in magnitudes (Fig. 4e) and maximum of 1 degree in angles (Fig. 4f) of state variables. Attack frequency and attack power might be strengthened by increasing  $\tau_{freq}$  and  $\tau_{loss}$  parameters in Algorithm 2 at risk of high detection by operator.

Having decided to input features  $[P_i, Q_i]_n \in \mathbb{R}^{5000 \times n \times 2}$  and output labels  $\mathbf{Y}_n \in \mathbb{R}^{5000}$  for  $n \in \{14, 118, 300\}$  bus test systems where 0 denotes honest and 1 denotes malicious samples of  $\mathbf{Y}_n$ , we partition the first 60% of the samples for training the proposed detectors, the next 20% for validating and tuning the hyper-parameter of the models, and the last 20% for evaluating the performances of the detectors. Then, we standardize each split separately, with a zero mean and a standard deviation of one, to have a faster and more stable learning process [39].

As a next step, we implement the GNN-based FDIA detector having a multi-layer Chebyshev graph convolution layer in its hidden layer and one dense layer on top of that as depicted in Fig. 3. We add a bias term and ReLU activation functions between graph convolutional layers and sigmoid activation functions at the last dense layer to increase the detector's nonlinear modeling ability [39]. As for weighted adjacency matrix  $\mathbf{W}$ , we use the magnitude of complex sparse Ybus matrix of the corresponding grid, which models the relation between nodes, determine the graph Laplacian  $L$  using (7) and scale it using (12) to obtain  $\tilde{L}$ .

All free unknown parameters defined in the model are computed by a supervised training using cross-entropy loss:

$$L(\hat{y}, W_\theta) = \frac{-1}{N} \sum_{n=1}^N y_i \log(\hat{y}_i) + (1 - y_i) \log(1 - \hat{y}_i), \quad (16)$$

over the training set where  $N$  denotes the number of samples

in the training set,  $W_\theta$  represents all trainable parameters  $\theta_l$  and  $b_l$  for  $1 \leq l \leq L$  along with  $W^L$  and  $b^L$  in the model, and  $y_i$  and  $\hat{y}_i$  stand for true and predicted class probability for sample  $i$ , respectively. Training samples are fed into the model as mini batches having 64 samples with 128 maximum number of epochs in addition to the early stopping where 16 epochs are tolerated without any improvement in the cross entropy loss of validation set. All the implementation was carried out in Python 3.8 using Pandapower [36], Sklearn [40], and Tensorflow [38] libraries on Intel i9-8950 HK CPU 2.90GHz with NVIDIA GeForce RTX 2070 GPU.

To evaluate the performance of proposed model in the binary classification task, we use true positive rate or detection rate (DR)  $DR = TP/(TP + FN)$  as probability of attack detection, false positive rate or false alarm rate (FA)  $FA = FP/(FP + TN)$  as probability of falsely alarming the system even though there is no attack, and the F-measure or F1 score  $F_1 = 2 * TP/(2TP + FP + FN)$  as the harmonic mean of the precision and sensitivity of classifier [39], where TP, FP, TN, and FN stand for true positives, false positives, true negatives and false negatives, respectively.

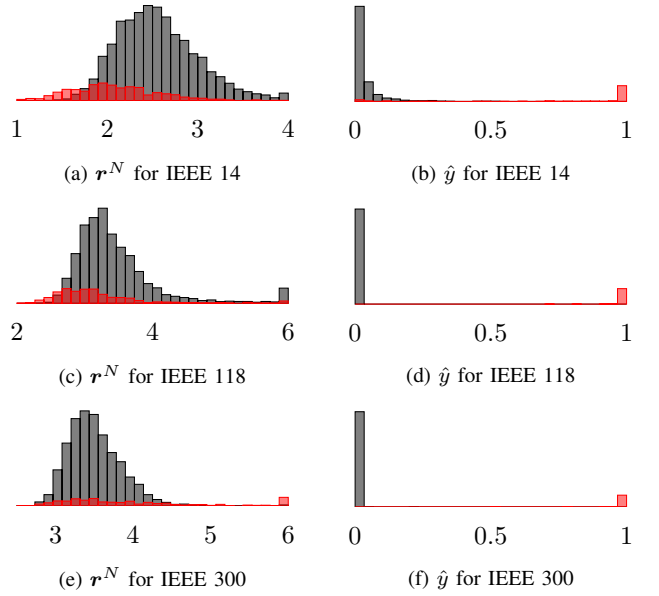


Fig. 5. Distributions of normalized residues  $r^N$  and predicted class probabilities  $\hat{y}$  for each IEEE test system having 14, 118, and 300 buses, respectively, computed on test dataset where black and red bars denote honest and malicious samples, respectively. GNN based detector transforms the class distributions so that they can be easily separated. In traditional BDD, in contrast, it is not possible to isolate the bad samples due to stealthy FDIA.

Predicted class probabilities  $\hat{y}$  obtained by GNN-based detector along with  $r^N$  values computed by the LNRT-based BDD system are given side-by-side for each test system in Fig. 5. Note that while it is almost impossible to separate honest and malicious samples by  $r^N$  due to intricate class distributions on the left side, the proposed GNN-based detector efficiently 'filters' malicious samples in its hidden layers and provides easily separable  $\hat{y}$  distributions. Please refer to Table I for detailed classification results.

#### D. Model scalability

Model scalability in terms of total number of parameters and prediction time is examined herein subsection. We first assess the total number of free trainable parameters in the proposed models. While each  $K$ -localized Chebyshev layer  $l$  having  $c_l$  channels for  $1 \leq l \leq L$  consists of  $K \cdot c_{l-1} \cdot c_l$  Chebyshev coefficients and  $c_l$  bias terms, the final dense layer assumes  $n \cdot c_L$  dense weights and a bias term. Thus, the total number of parameters in the model is given by:

$$K \sum_{l=1}^{l=L} ((c_{l-1} + 1) \times c_l) + n \cdot c_L + 1. \quad (17)$$

It can be seen from (17) that except for the last dense layer, the number of parameters in a GNN is free from bus size  $n$  and it linearly and independently scales with the neighborhood order  $K$ , previous layer's filter size  $c_{l-1}$  and its own filter size  $c_l$ . Second, we measure and save the prediction delays of each system. To fairly analyze how prediction time  $t$  and total number of parameters  $p$  change with the increasing bus size  $n$ , we fix the other variables at  $K = 3$ ,  $L = 3$ , and  $c_l = 32$  for each layer  $l$ . Fig. 6 demonstrates that models are linearly scalable in terms of  $n$ .

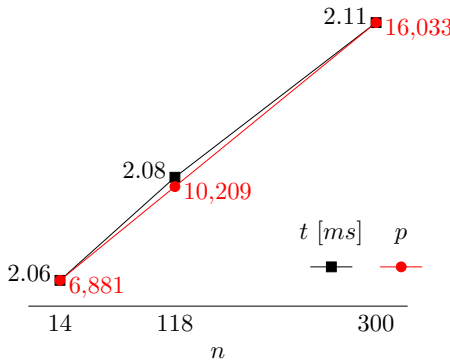


Fig. 6. Linear scalability of the proposed models in terms of prediction time  $t$  [ms] and total number of parameters  $p$ .

#### E. Visualization of how information spreads through layers

In this subsection, to explain and visualize how the proposed GNN-based detector distinguishes a malicious sample from a honest one, we examine the output of the filters from each layer of a trained network. To this end, first we arbitrarily select a node from the center region of the grid, for instance, bus 68 of the IEEE 118 bus system. Second, we randomly choose a honest sample  $s$  from the training data set and create a malicious sample  $\acute{s}$  by adding a point-wise attack to the bus 68 with a magnitude one to easily follow the spreading of this anomalous information through the hidden layers of the network. To focus on the anomaly, we calculate the difference of the Chebyshev filter outputs  $\delta^l = \acute{s}^l - s^l$  at each layer  $l$  for  $0 \leq l \leq 4$  including the input layer  $l = 0$ . Starting from  $\delta_0$ , the example filter output differences from each of the Chebyshev layers are depicted in Fig. 7. It can be clearly seen from Fig. 7 that each node transmits this anomalous data to its  $K$ -neighbors, where  $K$  is chosen as 3 for this network,

and the information advances in  $K$ -locality through each of the Chebyshev layers. The dense layer at the end of the model, in contrast, uses the anomalous features and decides its outputs by a sigmoid function. As expected,  $s^4 = 0$  and  $\acute{s}^4 = 1$  at the output of the model. In essence,  $K$ -localized Chebyshev filters of the proposed detector extract this spatial information through its GNN and dense layers to predict the probability of attacks for the input sample.

#### F. Comparison with Other Methods

To compare our GNN-based models with the available detectors, we also implement Decision Tree (DTC) [21], Support Vector (SVC) [17], Multi Layer Perceptron (MLP) [18], Recurrent Neural Network (RNN) [20], and Convolutional Neural Network (CNN) [19] based FDIA detectors. Since we do not have access to the data set of corresponding works, we train, validate and test these models similar to our proposed detector using our dataset.

DTC is a member of the non-parametric and supervised machine learning algorithms family aiming to create a multitude of decision rules on the input features to predict the class labels [41]. SVC, in contrast, tries to predict the hyperplane fitting the target variable by maximizing the margin and keeping the error within a threshold [42]. Therefore, only the support vectors residing in the margin contribute to the decision boundary and determine the error tolerance of the fitted hyperplane. MLP is a feed-forward type NN consisting of one input layer, one or more hidden layers, and one output layer. It is trained by using a backpropagation algorithm which iterates backwards the errors from the output layer to the lower layers, and feed-forwards the weight updates from the input layer to the higher layers [43]. Different from MLP, RNN is a NN that utilizes an internal memory component to remember its previous outputs to be used as next inputs which enables it to appropriately model sequential data [44]. CNN, on the contrary, is a regularized form of MLP where fully connected relations are replaced with shift invariant and weight shared convolution filters which allows it to better model the spatial and temporal correlations of the data [45].

The detection rate (DR), false alarm rate (FA), and F1 score of each model for each test system are given as percentages in Table I. Clearly, the LNR-based BDD system falls behind every other model due to non-separable class distributions of  $r^N$  values, as depicted in Fig. 5. For IEEE 14 and 118 bus systems, in particular, it simply predicts each sample as malicious, and this results in 100% FA rate. Non-NN based approaches such as DTC and SVM, in contrast, enhance the FA and perform better than BDD by an F1 score range between 72.43% - 95.50% due to their nonlinear modeling capabilities. The NN-based family surpasses the non-NN based models in general, except the MLP where it achieves comparable results with SVC. The RNN-based detector yields 83.0%, 98.61%, and 98.17% F1 score for IEEE 14, 118, and 300 bus systems, respectively. Only CNN and GNN based detectors reach the 0% FA rate. Nevertheless, GNN outperforms CNN models by 6.21%, 0.69%, and 2.73% in DR and by 3.65%, 0.34% and 1.38% in F1 for IEEE test cases with 14, 118, and 300 buses, respectively.

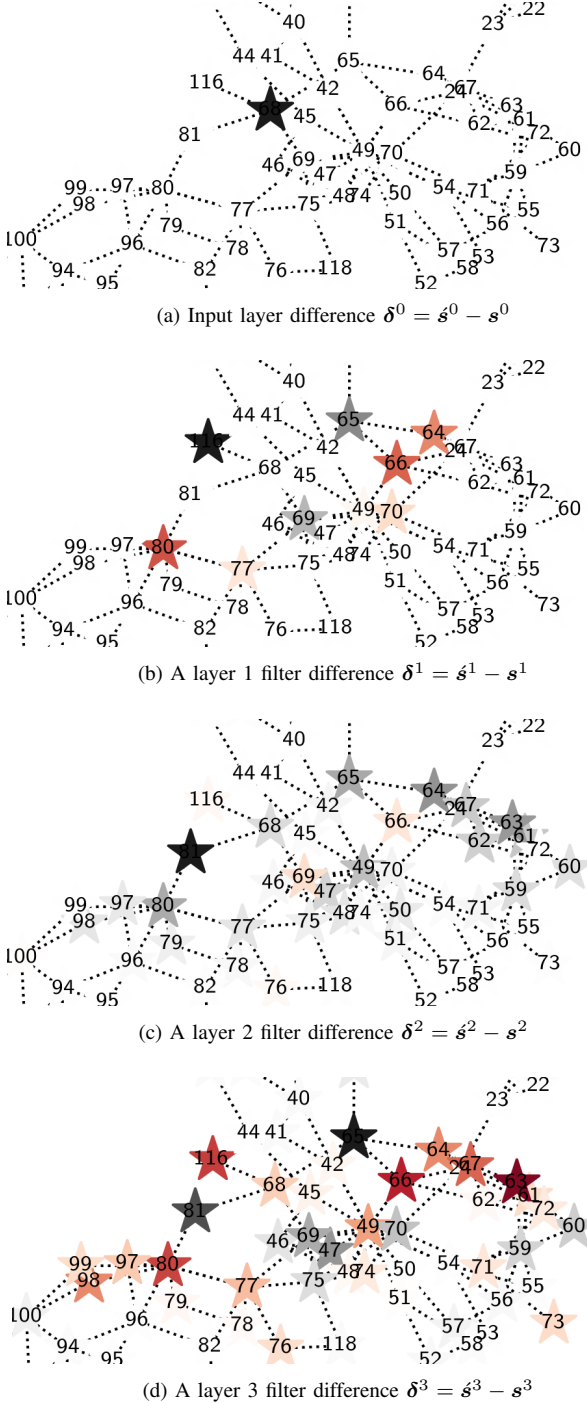


Fig. 7. Visualization of anomaly propagation through the layers of the proposed network. To better follow how the anomaly spreads, we plotted the signal differences at each layer. It can be clearly seen that each node sends information up to its  $K$ -neighbor in each filter and the message advances  $K$  nodes through each layer. Note that  $K$  is chosen 3 for this network in the training phase. For clarity, only affected area of the grid is depicted.

Our experiments point out that architectural differences in NN family play a vital role in terms of detection performance. MLP-based detectors tend to overfit the training data and fail to generalize due to its fully connected relationship between its units. RNNs, in contrast, can not achieve desired results since node values do not form a sequence type of data. Performance of CNN-based models comes after GNN due to their ability to

model the temporal and spatial relations of the input data in the Euclidean space, where the locality of the input features can be represented by regular linear grids such as in image or video data. Nevertheless, the inherent graph structure of power grid measurements can not be modeled in the Euclidean space except in trivial cases. As a matter of fact, graph data requires topology-aware models such as GNN to better reflect the adjacency relations of the measurement data.

TABLE I

COMPARISON OF DETECTOR PERFORMANCES IN TERMS OF DETECTION RATE (DR), FALSE ALARM (FA), AND F-MEASURE (F1) CLASSIFICATION METRICS FOR EACH IEEE TEST CASE SYSTEM WITH 14, 118, AND 300 BUSES. PROPOSED GNN BASED DETECTOR OUTPERFORMS ALL THE OTHER MODELS.

model	IEEE 14			IEEE 118			IEEE 300		
	DR	FA	F1	DR	FA	F1	DR	FA	F1
<b>BDD</b>	100.0	100.	25.33	100.0	100.	25.33	31.82	2.25	42.42
<b>DTC</b>	60.69	1.17	72.43	73.79	1.99	79.55	81.82	0.11	89.55
<b>SVC</b>	81.38	0.00	89.73	82.76	0.23	89.89	96.36	0.67	95.50
<b>MLP</b>	79.31	0.00	88.46	91.03	0.35	94.29	70.00	0.34	81.05
<b>RNN</b>	72.41	0.35	83.00	97.93	0.12	98.61	97.27	0.11	98.17
<b>CNN</b>	81.38	0.00	89.73	98.62	0.00	99.31	97.27	0.00	98.62
<b>GNN</b>	87.59	0.00	93.38	99.31	0.00	99.65	100.0	0.00	100.0

#### G. Tuning Model Hyperparameters

Traditional hyper-parameter tuning algorithms such as random search and grid search try to find the optimal parameters by randomly or sequentially sampling the parameters from the hyper-parameter space of the model and ignoring the results of previous trials. For example, even though any combination of a parameter set for a specific value of a parameter would fail to perform well regardless of the other parameters, these techniques might continue to run its trials with these specific values. Thereupon, selecting the optimal hyper parameters using random or grid search could be highly stagnant particularly for large hyper-parameter spaces. On the contrary, the Bayesian optimization technique considers performances of the past trials to better explore the parameter space. By focusing on more ‘promising’ regions of the parameters space in the light of its past experiences, it tries to select parameter combinations which give better validation performance. As a consequence of this informed navigation and sampling, it reduces the search time and offers better set of parameters which can lead to better model performance [46]. All model hyper-parameters are tuned using Bayesian optimization techniques, Sklearn [40] and Keras-tuner [47] Python libraries. Whereas the model fitting is performed on the training split of data, evaluation and optimal parameter selection are carried out on the validation split. After choosing the best hyper-parameters in 200 trials for each model, performances of the models having optimal parameters are assessed on the test splits, and results are saved. Please refer to Table II for the hyper-parameter set and Table III for the optimal hyper-parameters.

## V. CONCLUSION

In this paper, we addressed the detection of stealth FDIA in modern AC power grids. To that end, we first developed

TABLE II  
HYPER-PARAMETER SPACES FOR EACH MODEL FAMILY.

class	name	set
<b>BDD</b>	threshold	{0.01, 0.02, ..., 5.0}
<b>DTC</b>	criterion	{gini, entropy}
	depth	{8, 9, ..., 64}
	features	{0.1, 0.2, ..., 0.9}
	leaf	{1, 2, ..., 8}
<b>SVC</b>	C	{1e-6, 1e-5, ..., 1e+2},
	degree	{1, 2, ..., 5}
	gamma	{1e-6, 1e-5, ..., 1e+2}
	kernel	{linear, poly, rbf}
<b>NN</b>	layers	{1,2,3,4}
	units	{8, 16, ..., 64}
	activation	{relu, elu, sigmoid, tanh}
	optimizer	{adam, sgd, rmsprop}

TABLE III  
OPTIMAL MODEL HYPER-PARAMETERS FOR EACH MODEL AS A RESULT OF BAYESIAN HYPER-PARAMETER TUNING.

grid		threshold				
<b>IEEE 14</b>			0.88			
<b>IEEE 118</b>			2.08			
<b>IEEE 300</b>			4.22			
(a) BDD						
grid		criterion	depth	features	leaf	
<b>IEEE 14</b>		entropy	13	0.8	4	
<b>IEEE 118</b>		entropy	61	0.8	4	
<b>IEEE 300</b>		entropy	61	0.5	1	
(b) DT						
grid		C	degree	gamma	kernel	
<b>IEEE 14</b>		1e1	2	1e-1	poly	
<b>IEEE 118</b>		1e2	-	1e-3	rbf	
<b>IEEE 300</b>		1e-2	2	1e2	poly	
(c) SVC						
grid	model	layers	units	K	activation	optimizer
<b>IEEE 14</b>	<b>MLP</b>	2	56	-	elu	adam
	<b>RNN</b>	3	48	-	relu	adam
	<b>CNN</b>	3	56	2	relu	adam
	<b>GNN</b>	3	32	3	relu	adam
<b>IEEE 118</b>	<b>MLP</b>	2	40	-	elu	RMSprop
	<b>RNN</b>	3	48	-	relu	RMSprop
	<b>CNN</b>	3	56	2	relu	RMSprop
	<b>GNN</b>	3	40	3	relu	RMSprop
<b>IEEE 300</b>	<b>MLP</b>	2	24	-	relu	RMSprop
	<b>RNN</b>	3	32	-	relu	RMSprop
	<b>CNN</b>	3	24	2	relu	RMSprop
	<b>GNN</b>	3	16	3	relu	RMSprop
(d) NN						

a generic, locally applied, and stealth FDIA generation technique by solving a nonlinear non-convex optimization problem using SGD algorithm and made available the labeled data to the research community. Second, we proposed a scalable and real-time detection mechanism for FDIA by fusing the underlying graph topology of power grid and spatially correlated measurement data in the hidden layer of a GNN. Finally, we tested our algorithms on standard test beds such as IEEE 14, 118, and 300 bus systems and demonstrated that the proposed GNN detector surpasses the currently available methods in

literature by 6.21%, 0.69%, and 2.73% in detection rate and by 3.65%, 0.34% and 1.38% in F1 score, respectively.

## REFERENCES

- [1] K. R. Davis, K. L. Morrow, R. Bobba, and E. Heine, "Power flow cyber attacks and perturbation-based defense," in *2012 IEEE Third International Conference on Smart Grid Communications (SmartGridComm)*. IEEE, 2012, pp. 342–347.
- [2] S. Sridhar, A. Hahn, and M. Govindarasu, "Cyber-physical system security for the electric power grid," *Proceedings of the IEEE*, vol. 100, no. 1, pp. 210–224, 2011.
- [3] G. B. Giannakis, V. Kekatos, N. Gatsis, S.-J. Kim, H. Zhu, and B. F. Wollenberg, "Monitoring and optimization for power grids: A signal processing perspective," *IEEE Signal Processing Magazine*, vol. 30, no. 5, pp. 107–128, 2013.
- [4] A. Abur and A. Expósito, *Power System State Estimation: Theory and Implementation*, ser. Power Engineering (Willis). CRC Press, 2004. [Online]. Available: [https://books.google.com/books?id=NQhbtFC6\\_40C](https://books.google.com/books?id=NQhbtFC6_40C)
- [5] H. He and J. Yan, "Cyber-physical attacks and defences in the smart grid: a survey," *IET Cyber-Physical Systems: Theory & Applications*, vol. 1, no. 1, pp. 13–27, 2016.
- [6] G. Liang, J. Zhao, F. Luo, S. R. Weller, and Z. Y. Dong, "A review of false data injection attacks against modern power systems," *IEEE Transactions on Smart Grid*, vol. 8, no. 4, pp. 1630–1638, 2016.
- [7] Y. Liu, P. Ning, and M. K. Reiter, "False data injection attacks against state estimation in electric power grids," *ACM Transactions on Information and System Security (TISSEC)*, vol. 14, no. 1, pp. 1–33, 2011.
- [8] P.-Y. Chen, S. Yang, J. A. McCann, J. Lin, and X. Yang, "Detection of false data injection attacks in smart-grid systems," *IEEE Communications Magazine*, vol. 53, no. 2, pp. 206–213, 2015.
- [9] O. Kosut, L. Jia, R. J. Thomas, and L. Tong, "Malicious data attacks on the smart grid," *IEEE Transactions on Smart Grid*, vol. 2, no. 4, pp. 645–658, 2011.
- [10] Y. Huang, J. Tang, Y. Cheng, H. Li, K. A. Campbell, and Z. Han, "Real-time detection of false data injection in smart grid networks: An adaptive cusum method and analysis," *IEEE Systems Journal*, vol. 10, no. 2, pp. 532–543, 2014.
- [11] E. Drayer and T. Routhenberg, "Detection of false data injection attacks in smart grids based on graph signal processing," *IEEE Systems Journal*, 2019.
- [12] J. Duan, W. Zeng, and M.-Y. Chow, "Resilient distributed dc optimal power flow against data integrity attack," *IEEE Transactions on Smart Grid*, vol. 9, no. 4, pp. 3543–3552, 2016.
- [13] M. G. Kallitsis, S. Bhattacharya, S. Stoev, and G. Michailidis, "Adaptive statistical detection of false data injection attacks in smart grids," in *2016 IEEE Global Conference on Signal and Information Processing (GlobalSIP)*. IEEE, 2016, pp. 826–830.
- [14] M. N. Kurt, Y. Yilmaz, and X. Wang, "Real-time detection of hybrid and stealthy cyber-attacks in smart grid," *IEEE Transactions on Information Forensics and Security*, vol. 14, no. 2, pp. 498–513, 2018.
- [15] ———, "Distributed quickest detection of cyber-attacks in smart grid," *IEEE Transactions on Information Forensics and Security*, vol. 13, no. 8, pp. 2015–2030, 2018.
- [16] J. Hao, E. Kang, J. Sun, Z. Wang, Z. Meng, X. Li, and Z. Ming, "An adaptive markov strategy for defending smart grid false data injection from malicious attackers," *IEEE Transactions on Smart Grid*, vol. 9, no. 4, pp. 2398–2408, 2016.
- [17] M. Esmalifalak, L. Liu, N. Nguyen, R. Zheng, and Z. Han, "Detecting stealthy false data injection using machine learning in smart grid," *IEEE Systems Journal*, vol. 11, no. 3, pp. 1644–1652, 2014.
- [18] E. M. Ferragut, J. Laska, M. M. Olama, and O. Ozmen, "Real-time cyber-physical false data attack detection in smart grids using neural networks," in *2017 International Conference on Computational Science and Computational Intelligence (CSCI)*. IEEE, 2017, pp. 1–6.
- [19] D. Wang, X. Wang, Y. Zhang, and L. Jin, "Detection of power grid disturbances and cyber-attacks based on machine learning," *Journal of Information Security and Applications*, vol. 46, pp. 42–52, 2019.
- [20] S. Binna, S. R. Kuppannagari, D. Engel, and V. K. Prasanna, "Subset level detection of false data injection attacks in smart grids," in *2018 IEEE Conference on Technologies for Sustainability (SusTech)*. IEEE, 2018, pp. 1–7.
- [21] K. Vimalkumar and N. Radhika, "A big data framework for intrusion detection in smart grids using apache spark," in *2017 International Conference on Advances in Computing, Communications and Informatics (ICACCI)*. IEEE, 2017, pp. 198–204.

[22] E. Drayer and T. Routhenberg, "Detection of false data injection attacks in power systems with graph fourier transform," in *2018 IEEE Global Conference on Signal and Information Processing (GlobalSIP)*. IEEE, 2018, pp. 890–894.

[23] R. Ramakrishna and A. Scaglione, "Detection of false data injection attack using graph signal processing for the power grid," in *2019 IEEE Global Conference on Signal and Information Processing (GlobalSIP)*. IEEE, 2019, pp. 1–5.

[24] R. Deng, G. Xiao, and R. Lu, "Defending against false data injection attacks on power system state estimation," *IEEE Transactions on Industrial Informatics*, vol. 13, no. 1, pp. 198–207, 2015.

[25] L. Liu, M. Esmalifalak, Q. Ding, V. A. Emesih, and Z. Han, "Detecting false data injection attacks on power grid by sparse optimization," *IEEE Transactions on Smart Grid*, vol. 5, no. 2, pp. 612–621, 2014.

[26] A. S. Musleh, G. Chen, and Z. Y. Dong, "A survey on the detection algorithms for false data injection attacks in smart grids," *IEEE Transactions on Smart Grid*, vol. 11, no. 3, pp. 2218–2234, 2019.

[27] Y. LeCun, Y. Bengio, and G. Hinton, "Deep learning," *nature*, vol. 521, no. 7553, pp. 436–444, 2015.

[28] D. Owerko, F. Gama, and A. Ribeiro, "Optimal power flow using graph neural networks," in *ICASSP 2020-2020 IEEE International Conference on Acoustics, Speech and Signal Processing (ICASSP)*. IEEE, 2020, pp. 5930–5934.

[29] E. Handschin, F. C. Schweppe, J. Kohlas, and A. Fiechter, "Bad data analysis for power system state estimation," *IEEE Transactions on Power Apparatus and Systems*, vol. 94, no. 2, pp. 329–337, 1975.

[30] P. Bojanowski, A. Joulin, D. Lopez-Paz, and A. Szlam, "Optimizing the latent space of generative networks," *arXiv preprint arXiv:1707.05776*, 2017.

[31] D. I. Shuman, S. K. Narang, P. Frossard, A. Ortega, and P. Vandergheynst, "The emerging field of signal processing on graphs: Extending high-dimensional data analysis to networks and other irregular domains," *IEEE signal processing magazine*, vol. 30, no. 3, pp. 83–98, 2013.

[32] F. R. Chung and F. C. Graham, *Spectral graph theory*. American Mathematical Soc., 1997, no. 92.

[33] A. Ortega, P. Frossard, J. Kovačević, J. M. Moura, and P. Vandergheynst, "Graph signal processing: Overview, challenges, and applications," *Proceedings of the IEEE*, vol. 106, no. 5, pp. 808–828, 2018.

[34] M. Defferrard, X. Bresson, and P. Vandergheynst, "Convolutional neural networks on graphs with fast localized spectral filtering," in *Advances in Neural Information Processing Systems (NIPS)*, 2016.

[35] J. C. Mason and D. C. Handscomb, *Chebyshev polynomials*. CRC press, 2002.

[36] L. Thurner, A. Scheidler, F. Schäfer, J.-H. Menke, J. Dollichon, F. Meier, S. Meinecke, and M. Braun, "pandapower—an open-source python tool for convenient modeling, analysis, and optimization of electric power systems," *IEEE Transactions on Power Systems*, vol. 33, no. 6, pp. 6510–6521, 2018.

[37] The Electric Reliability Council of Texas (ERCOT). Backcasted (actual) load profiles - historical. (2020, May 10). [Online]. Available: <http://www.ercot.com/mktinfo/loadprofile/alp/>

[38] M. Abadi, A. Agarwal, P. Barham, E. Brevdo, Z. Chen, C. Citro, G. S. Corrado, A. Davis, J. Dean, M. Devin, S. Ghemawat, I. Goodfellow, A. Harp, G. Irving, M. Isard, Y. Jia, R. Jozefowicz, L. Kaiser, M. Kudlur, J. Levenberg, D. Mané, R. Monga, S. Moore, D. Murray, C. Olah, M. Schuster, J. Shlens, B. Steiner, I. Sutskever, K. Talwar, P. Tucker, V. Vanhoucke, V. Vasudevan, F. Viégas, O. Vinyals, P. Warden, M. Wattenberg, M. Wicke, Y. Yu, and X. Zheng, "TensorFlow: Large-scale machine learning on heterogeneous systems," 2015, software available from tensorflow.org. [Online]. Available: <https://www.tensorflow.org/>

[39] C. M. Bishop, *Pattern recognition and machine learning*. Springer, 2006.

[40] F. Pedregosa, G. Varoquaux, A. Gramfort, V. Michel, B. Thirion, O. Grisel, M. Blondel, P. Prettenhofer, R. Weiss, V. Dubourg, J. Vanderplas, A. Passos, D. Cournapeau, M. Brucher, M. Perrot, and E. Duchesnay, "Scikit-learn: Machine learning in Python," *Journal of Machine Learning Research*, vol. 12, pp. 2825–2830, 2011.

[41] S. R. Safavian and D. Landgrebe, "A survey of decision tree classifier methodology," *IEEE transactions on systems, man, and cybernetics*, vol. 21, no. 3, pp. 660–674, 1991.

[42] D. Lee and J. Lee, "Domain described support vector classifier for multi-classification problems," *Pattern Recognition*, vol. 40, no. 1, pp. 41–51, 2007.

[43] S. K. Pal and S. Mitra, "Multilayer perceptron, fuzzy sets, and classification," *IEEE Transactions on Neural Networks*, vol. 3, no. 5, pp. 683–697, 1992.

[44] P. Rodriguez, J. Wiles, and J. L. Elman, "A recurrent neural network that learns to count," *Connection Science*, vol. 11, no. 1, pp. 5–40, 1999.

[45] J. S. Denker, W. Gardner, H. P. Graf, D. Henderson, R. E. Howard, W. Hubbard, L. D. Jackel, H. S. Baird, and I. Guyon, "Neural network recognizer for hand-written zip code digits," in *Advances in neural information processing systems*, 1989, pp. 323–331.

[46] E. Brochu, V. M. Cora, and N. De Freitas, "A tutorial on bayesian optimization of expensive cost functions, with application to active user modeling and hierarchical reinforcement learning," *arXiv preprint arXiv:1012.2599*, 2010.

[47] T. O'Malley, E. Bursztein, J. Long, F. Chollet, H. Jin, L. Invernizzi et al., "Keras Tuner," <https://github.com/keras-team/keras-tuner>, 2019.